

# Sonochemical preparation of nanosized amorphous Fe-Ni alloys<sup>a)</sup>

K. V. P. M. Shafi and A. Gedanken<sup>b)</sup>

Department of Chemistry, Bar-Ilan University, Ramat-Gan 52900, Israel

R. B. Goldfarb

Electromagnetic Technology Division, National Institute of Standards and Technology, Boulder, Colorado 80303

I. Felner

Racah Institute of Physics, Hebrew University, Jerusalem 91904, Israel

(Received 4 October 1996; accepted for publication 13 February 1997)

Nanosized amorphous alloy powders of Fe<sub>20</sub>Ni<sub>80</sub>, Fe<sub>40</sub>Ni<sub>60</sub>, and Fe<sub>60</sub>Ni<sub>40</sub> were prepared by sonochemical decomposition of solutions of volatile organic precursors, Fe(CO)<sub>5</sub> and Ni(CO)<sub>4</sub> in decalin, under an argon pressure of 100 to 150 kPa at 273 K. Magnetic susceptibility of Fe<sub>40</sub>Ni<sub>60</sub> and Fe<sub>60</sub>Ni<sub>40</sub> indicates blocking temperatures of 35 K and a magnetic particle size of about 6 nm. Thermogravimetric measurements of Fe<sub>20</sub>Ni<sub>80</sub> give Curie temperatures of 322 °C for amorphous and 550 °C for crystallized forms. Differential scanning calorimetry exhibits an endothermic transition at 335 °C from a combination of the magnetic phase transition and alloy crystallization. The Mössbauer spectrum of crystallized Fe<sub>20</sub>Ni<sub>80</sub> shows a sextet pattern with a hyperfine field of 25.04 T. © 1997 American Institute of Physics. [S0021-8979(97)06310-X]

## I. INTRODUCTION

Amorphous alloys—metallic glasses or glassy metals obtained by rapid quenching of the melt—lack the long-range atomic order of their crystalline counterparts. Because of their unique electronic, magnetic, and corrosion-resistant properties,<sup>1-4</sup> they are of technological importance. Ferromagnetic amorphous alloys containing Fe and Co have excellent soft magnetic properties equivalent or superior to those of conventional materials. Some uses include magnetic recording heads and power transformer cores.<sup>5</sup> An important feature of the Fe-Ni alloy system is its structural evolution, with a change from bcc for the Fe-rich alloy to fcc for the alloy with larger Ni content. Much attention has focused on its Invar (low thermal expansion) behavior.<sup>6,7</sup>

In this paper, we discuss the sonochemical synthesis and the characterization of nanosized amorphous Fe<sub>x</sub>Ni<sub>1-x</sub> alloy particles. Acoustic cavitation (the formation, growth, and subsequent implosive collapse of a bubble in an ultrasonically irradiated liquid) generates a transient localized hot spot with an effective temperature of 5000 K and a submicrosecond lifetime.<sup>8-10</sup> The rapid cavitation cooling rate (>10<sup>9</sup> K/s) is much greater than that obtained by conventional melt spinning<sup>11</sup> (10<sup>5</sup> to 10<sup>6</sup> K/s).

The foremost criterion for achieving good sonochemical yield is that the precursor should be volatile, because the primary sonochemical reaction site is the vapor inside the cavitation bubbles.<sup>12</sup> Second, the solvent vapor pressure should be lower at the sonochemical temperature, since solvent vapor inside the bubble reduces the collapse efficiency. Suslick *et al.* have employed this new sonochemical method for the preparation of nanosized amorphous powders of Fe,

Co, and their alloys,<sup>13-16</sup> and the metal carbide Mo<sub>2</sub>C.<sup>17</sup> They showed that, by using polymeric ligands like polyvinylpyrrolidone (PVP) or oxide supports (alumina or silica), these nanosized clusters can be trapped as colloids or supported catalysts, respectively.<sup>18</sup>

We have reported the preparation of amorphous Ni powder by sonochemical decomposition of nickel tetracarbonyl Ni(CO)<sub>4</sub> as neat liquid or solution in decalin (decahydronaphthalene).<sup>19</sup> We showed that we could control the particle size of amorphous Fe by varying the precursor, iron pentacarbonyl Fe(CO)<sub>5</sub>, concentration in decalin during sonication.<sup>20</sup> We also reported the preparation of amorphous Fe<sub>2</sub>O<sub>3</sub> by sonication of neat Fe(CO)<sub>5</sub> or its solution in decalin in air.<sup>21</sup>

## II. EXPERIMENTAL PROCEDURE

We used iron pentacarbonyl without further purification, but distilled nickel tetracarbonyl before use. Nickel tetracarbonyl is a highly poisonous liquid with a high vapor pressure. It is very sensitive to air and moisture, so care should be taken in handling it. Pentane and decalin were dried with sodium metal or a no. 4 molecular sieve and stored in a glove box. We degassed the precursor solution by purging with high purity argon (< 10 ppm O<sub>2</sub>) prior to sonication.

We prepared the Fe-Ni alloy by ultrasonic irradiation of the solution of Fe(CO)<sub>5</sub> and Ni(CO)<sub>4</sub> in decalin at 273 K, under 100 to 150 kPa (1 to 1.5 atm) argon, with a high intensity ultrasonic probe (Sonics and Materials, model VC-600, 1.25 cm Ti horn, 20 kHz, 100 W/cm<sup>2</sup>). After 3 h of irradiation, a black powder was obtained which was centrifuged and washed with dry pentane in a glovebox. Centrifuging and washing were repeated at least five times, and the product was then dried under vacuum. We prepared the different compositions of Fe-Ni (Fe<sub>20</sub>Ni<sub>80</sub>, Fe<sub>40</sub>Ni<sub>60</sub>, and Fe<sub>60</sub>Ni<sub>40</sub>) by varying the molar concentration of the precursors in solution.

<sup>a)</sup>Part of this work was presented at the International Alloy Conference (IAC<sub>1</sub>), Athens, Greece, June 1996.

<sup>b)</sup>Author to whom correspondence should be sent. Electronic mail: gedanken@ashur.cc.biu.ac.il

Cu  $K_{\alpha}$  radiation,  $\lambda=0.15418$  nm, was used for powder x-ray diffraction. We characterized the powder using scanning electron microscopy (SEM), energy dispersive x-ray analysis (EDX), and transmission electron microscopy (TEM). Magnetic data were obtained with a magnetometer based on a superconducting quantum interference device (SQUID). Specific surface area was measured on a surface area analyzer using the Brauner–Emmet–Teller (BET) method.

Mössbauer spectroscopy was carried out with a conventional constant-acceleration spectrometer with a  $1.85 \times 10^9$  Bq (50 mCi)  $^{57}\text{Co}:\text{Rh}$  source. Portions of the samples were annealed in evacuated quartz tubes at 210 °C for 10 h and at 420 °C for 5 h. Mössbauer spectroscopy at room temperature was performed for all samples, and the spectrum of the sample annealed at 420 °C was least-squares fitted. The isomer shift value is relative to iron metal.

Thermogravimetric (TG) magnetic measurements were made using a balance and a small permanent magnet. Differential scanning calorimetry (DSC) thermograms were obtained using a heating rate of 10 °C/min under flowing, pure nitrogen (50 ml/min). To avoid oxidation, all sample preparation and transfers were done in a glovebox. During the measurements, the samples were exposed to inert gases only.

### III. RESULTS AND DISCUSSION

Alloy compositions were determined by elemental and EDX analyses. Since the atomic numbers of Ni and Fe are similar, the ratio of the x-ray intensities from these elements approximate the alloy composition. Since the  $<25$  nm size of these particles is much smaller than the 100 nm free path for x-ray transmission through solids, the x-ray intensities need not be corrected for absorption and fluorescence.

The elemental analyses show that the amorphous alloy powders have over 95% metal by mass, with carbon ( $<3\%$ ) and oxygen ( $<2\%$ ).<sup>15</sup> The presence of carbon and oxygen is presumably a result of the decomposition of alkane solvents or adsorbed CO during ultrasonication. These elements probably play an important role in stabilizing the amorphous structure.

The amorphous nature of the alloy particles was confirmed by various techniques, including SEM, TEM, electron microdiffraction, and x-ray diffraction. Scanning microscopy of the alloy powder showed conchoidal fractures typical in noncrystalline materials.<sup>13</sup> The TEM image (Fig. 1) shows no evidence of crystallite formation and shows that the alloy particles are agglomerates of small particles with overall diameters  $<25$  nm. Most of the particles are aggregated in a spongelike form, so it is difficult to determine the particle size exactly. TEM microdiffraction of the alloy particles shows only diffuse rings characteristic of amorphous materials.

Figure 2 shows the x-ray diffraction patterns for amorphous  $\text{Fe}_{20}\text{Ni}_{80}$  as well as the heated samples of  $\alpha\text{-Fe}$ ,  $\gamma\text{-Ni}$ ,  $\text{Fe}_{20}\text{Ni}_{80}$ ,  $\text{Fe}_{40}\text{Ni}_{60}$ , and  $\text{Fe}_{60}\text{Ni}_{40}$ . The x-ray diffractogram of the amorphous solid shows a broad peak centered around a  $2\theta$  value of 44.6°. No sharp diffraction patterns characteristic of crystalline phases appear. After heat treatment under pure argon ( $<10$  ppm  $\text{O}_2$ ) at 450 °C for 5 h to

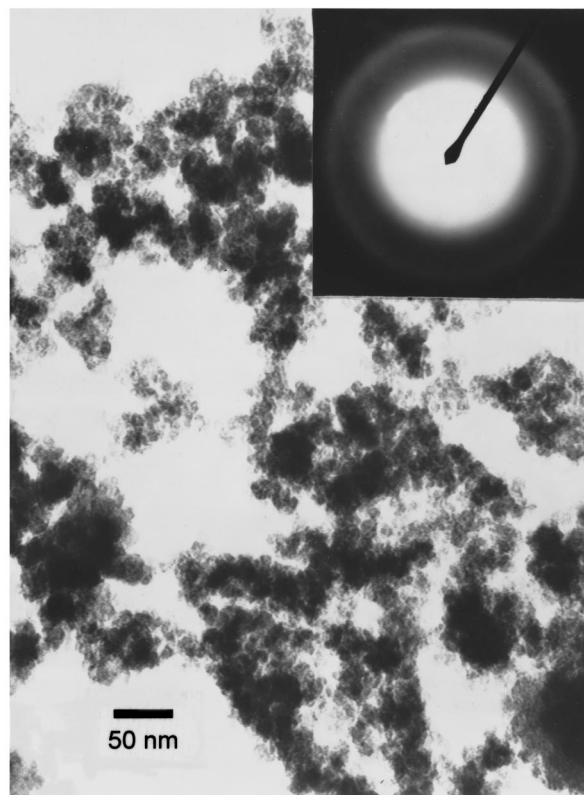


FIG. 1. Transmission electron microscope image of amorphous  $\text{Fe}_{20}\text{Ni}_{80}$  and microdiffraction pattern (inset).

induce crystallization, lines characteristic of  $\gamma\text{-Ni}$  (fcc) start to appear. Lack of any feature at  $2\theta$  values of 65.2° and 82.3° ( $\lambda=0.15418$  nm), which are the expected positions of bcc  $\alpha\text{-Fe}$  (200) and (211), confirm that the Fe and Ni become alloyed, rather than forming separate grains. Even for the higher concentration of Fe in  $\text{Fe}_{60}\text{Ni}_{40}$ , the phase is still fcc of  $\gamma\text{-Ni}$  and not bcc of  $\alpha\text{-Fe}$ . This is in accordance with the reported equilibrium structural phase diagram of Fe–Ni binary alloys<sup>22</sup> prepared by the conventional method and thermal treatment.

The Mössbauer spectrum for the amorphous  $\text{Fe}_{20}\text{Ni}_{80}$  alloy at room temperature, after heating at 420 °C for 5 h, is shown in Fig. 3. A well defined sextet shows that the local environment of the Fe is ordered by the annealing process. The hyperfine parameters at 300 K are: isomer shift  $\text{IS}=0.044(1)$  mm/s, effective quadrupole interaction  $\text{QE}=-0.06(2)$  mm/s, and effective magnetic hyperfine field  $H_{\text{eff}}=25.04$  T. A sextet pattern is not obtained in the as-prepared, amorphous samples because, at 300 K, they are superparamagnetic and above the blocking temperature (see below).

The sextet pattern in the Mössbauer spectrum with a hyperfine field of 25.04 T is additional evidence for the formation of the Fe–Ni alloy, rather than separate Fe and Ni clusters, in the particles. The hyperfine field is near the value for bulk  $\text{Fe}_{20}\text{Ni}_{80}$  alloy ( $\approx 28.2$  T),<sup>23</sup> the slight reduction in value can be justified if we consider that the magnetic hyperfine field of nanoparticles may be smaller than that of the

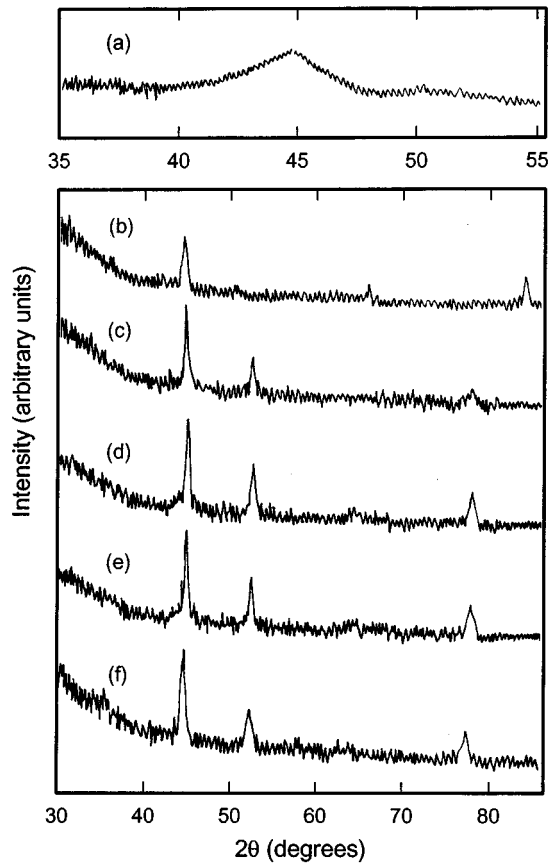


FIG. 2. X-ray diffraction patterns for (a) amorphous  $\text{Fe}_{20}\text{Ni}_{80}$ , (b) crystalline  $\alpha$ -Fe, (c) crystalline  $\gamma$ -Ni, (d) crystalline  $\text{Fe}_{20}\text{Ni}_{80}$ , (e) crystalline  $\text{Fe}_{40}\text{Ni}_{60}$ , (f) crystalline  $\text{Fe}_{60}\text{Ni}_{40}$ .

corresponding bulk material.<sup>24</sup> The magnetic hyperfine field of pure metallic iron is 33.0 T.

The BET specific surface areas per unit mass of the amorphous and crystallized (heated) samples of  $\alpha$ -Fe,  $\gamma$ -Ni,  $\text{Fe}_{20}\text{Ni}_{80}$ ,  $\text{Fe}_{40}\text{Ni}_{60}$ , and  $\text{Fe}_{60}\text{Ni}_{40}$  are given in Table I. The decrease in surface area of upon crystallization is due to the increase in agglomeration because of sintering that occurs on heating.

Magnetic susceptibility (Fig. 4) was measured as a function of increasing temperature after zero-field cooling (ZFC) and field cooling (FC) in a dc field of 1 mT. The Fe-Ni alloy

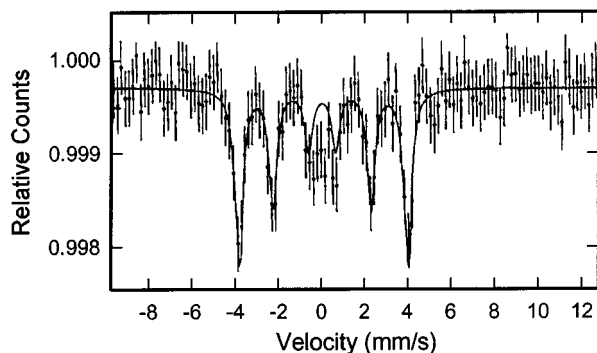


FIG. 3. Mössbauer spectrum measured at 300 K of  $\text{Fe}_{20}\text{Ni}_{80}$  heated at 420 °C for 5 h. Note the well defined sextet pattern.

TABLE I. Specific surface area per unit mass of amorphous and crystallized (heated) samples of  $\alpha$ -Fe,  $\gamma$ -Ni,  $\text{Fe}_{20}\text{Ni}_{80}$ ,  $\text{Fe}_{40}\text{Ni}_{60}$ , and  $\text{Fe}_{60}\text{Ni}_{40}$ .

Sample	Surface area ( $\text{m}^2/\text{g}$ )	
	Amorphous	Crystalline
$\alpha$ -Fe	110	35
$\gamma$ -Ni	76	25
$\text{Fe}_{20}\text{Ni}_{80}$	52	23
$\text{Fe}_{40}\text{Ni}_{60}$	35	18
$\text{Fe}_{60}\text{Ni}_{40}$	68	34

particles are superparamagnetic. Both  $\text{Fe}_{40}\text{Ni}_{60}$  and  $\text{Fe}_{60}\text{Ni}_{40}$  exhibit average blocking temperatures of 35 K with respect to a measurement time of about 10 min required to scan the relevant temperature range. The broad susceptibility peaks indicate a distribution in particle size. Irreversibility occurs below 200–250 K. Alternating field susceptibility in 1  $\mu\text{T}$  at 10 and 1000 Hz show blocking temperatures of 41 and 45 K for  $\text{Fe}_{40}\text{Ni}_{60}$  and about 51 and 55 K for  $\text{Fe}_{60}\text{Ni}_{40}$ . All blocking temperatures and measurement time constants are consistent with magnetic particle diameters on the order of 6 nm (about one fourth the average agglomerate size) if we assume typical uniaxial anisotropies of  $10^5 \text{ J}/\text{m}^3$ . As expected, the alloy with higher Fe content has a larger susceptibility. Owing to the random alignment of anisotropic particles with a distribution of sizes and moments, along with some irreversibility, a Curie law is not followed exactly.

Figure 5 shows the result of a magnetic force measurement, obtained with a thermogravimetric balance, on amorphous  $\text{Fe}_{20}\text{Ni}_{80}$  alloy powder. The percent change in weight is plotted as a function of increasing temperature. The amorphous powder has a Curie temperature  $T_C$  of 322 °C, followed by a higher  $T_C$  at 550 °C associated with the crystalline form of the alloy.<sup>22</sup>

The DSC measurement of amorphous  $\text{Fe}_{20}\text{Ni}_{80}$ , plotted as specific power in watts per gram, is shown in Fig. 6. Exothermic transitions would have positive peaks. Surprisingly, we did not observe an exothermic peak characteristic

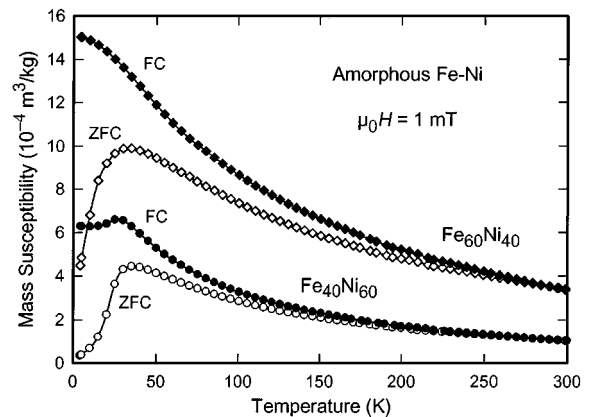


FIG. 4. Mass susceptibility of two amorphous bimetallic Fe-Ni alloy powders as a function of increasing temperature after zero-field cooling (ZFC) and field cooling (FC). To convert mass susceptibility from  $\text{m}^3/\text{kg}$  to  $\text{emu}/\text{g}$ , multiply by  $1000/4\pi$ .

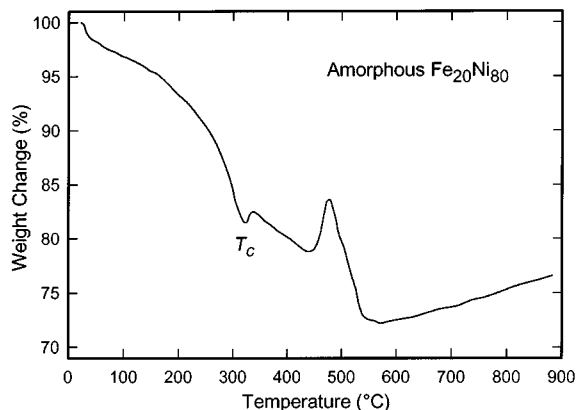


FIG. 5. Thermogravimetric measurement of weight change in amorphous  $\text{Fe}_{20}\text{Ni}_{80}$  alloy powder. The dip at  $322^\circ\text{C}$  corresponds to the Curie temperature  $T_C$ ; the one at  $550^\circ\text{C}$  corresponds to  $T_C$  of the crystalline form.

of crystallization. Rather, we measured two endotherms with peak minima at  $180$  and  $335^\circ\text{C}$ .

To check whether these endothermic peaks are due to the desorption of materials from the alloy surface, we performed a mass spectrometric study. We heated the  $\text{Fe}_{20}\text{Ni}_{80}$  alloy at a rate of  $30^\circ\text{C}/\text{min}$  and recorded the total ion current as a function of temperature. A peak was observed at about  $200^\circ\text{C}$  (somewhat higher than the first endothermic peak because of the higher heating rate). The total ion peak was mass-resolved into peaks of pentane and decalin as well as an unexplained mass of  $128$  unified atomic mass units (u). This indication that Fe–Ni alloys prepared by ultrasonication contain strongly adsorbed hydrocarbon solvents pentane and decalin is expected because the nanostructured amorphous materials are highly porous, as seen on TEM micrographs.

To verify this, we ran the DSC of  $\text{Fe}_{20}\text{Ni}_{80}$  in two scans. The first involved heating to  $220^\circ\text{C}$  at a rate of  $10^\circ\text{C}/\text{min}$ . After the sample was cooled to room temperature, it was heated to  $500^\circ\text{C}$  at a rate of  $10^\circ\text{C}/\text{min}$ . The endothermic peak at  $180^\circ\text{C}$  nearly vanished in the second DSC scan. We are thus satisfied that this first endothermic peak is due to the desorption of the solvents.

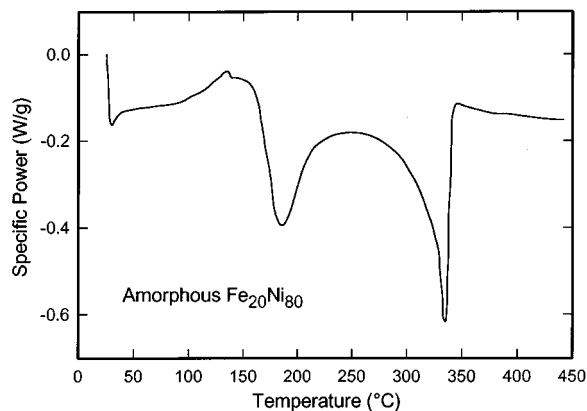


FIG. 6. Differential scanning calorimetry (DSC) curves of specific power for amorphous  $\text{Fe}_{20}\text{Ni}_{80}$  powder. The endothermic peak minimum near  $200^\circ\text{C}$  results from the desorption of solvents; the one at  $335^\circ\text{C}$  is associated with the Curie transition and alloy crystallization.

The second endothermic peak in Fig. 6 corresponds to a convolution of the magnetic Curie transition ( $T_C = 322^\circ\text{C}$ ) and the amorphous-to-crystalline transition upon heating (expected around  $325\text{--}350^\circ\text{C}$ ). The endothermicity of the magnetic transition presumably dominates over the usual exothermicity of the amorphous-to-crystalline transition, resulting in a net negative peak near  $335^\circ\text{C}$  in Fig. 6. A more detailed study is required, however, since the thermal behavior of the alloy particles is very sensitive to the history of sample preparation, the annealing temperature, and the heating rate.

#### IV. CONCLUDING REMARKS

Sonochemical decomposition of solutions of volatile organic precursors,  $\text{Fe}(\text{CO})_5$  and  $\text{Ni}(\text{CO})_4$  in decalin at  $273\text{ K}$ , under an argon pressure of  $100$  to  $150\text{ kPa}$  ( $1$  to  $1.5\text{ atm}$ ), yield amorphous, nanosized Fe–Ni alloy particles. The composition of these alloy particles can be controlled by varying the initial precursor concentration in solution. We have noticed that the sonochemical efficiency for the decomposition is less for  $\text{Fe}(\text{CO})_5$  than for  $\text{Ni}(\text{CO})_4$ , so it is necessary to use an initial excess of  $\text{Fe}(\text{CO})_5$  (about three times the concentration of  $\text{Ni}(\text{CO})_4$ ) to get the desired alloy composition. The poor reactivity of  $\text{Fe}(\text{CO})_5$  compared to  $\text{Ni}(\text{CO})_4$  can be traced to its lower vapor pressure. For example, at  $293\text{ K}$ , the vapor pressure is  $44.3\text{ kPa}$  ( $332\text{ Torr}$ ) for  $\text{Ni}(\text{CO})_4$ , whereas it is only  $2.8\text{ kPa}$  ( $21\text{ Torr}$ ) for  $\text{Fe}(\text{CO})_5$ .

Flint and Suslick<sup>9</sup> found that there are two regions of sonochemical reactivity in ultrasonically irradiated liquids, one corresponding to the gas phase within the collapsing cavity and the other to a thin liquid layer immediately surrounding the collapsing cavity. The observed dependence of sonochemical reactivity on metal carbonyl vapor pressure is expected for reactions occurring in the gas phase. As the precursor's vapor pressure increases, its concentration within the gas-phase cavity increases linearly, thus increasing the observed sonochemical reaction rate. Further, on sonochemical decomposition,  $\text{Fe}(\text{CO})_5$  yields  $\text{Fe}_3(\text{CO})_{12}$  in addition to metallic Fe.<sup>25</sup>

Initial tests to check the catalytic activity of these amorphous Fe–Ni alloy particles on the decomposition of hydrogen peroxide ( $10\%$   $\text{H}_2\text{O}_2$  aqueous solution) show that these are better catalysts than the parent amorphous Fe or Ni powders by a factor of  $3$ .

#### ACKNOWLEDGMENT

This research was supported by Grant No.  $94\text{-}00230$  from the U.S.–Israel Binational Science Foundation (BSF), Jerusalem. We thank the Ministry of Science and Arts, Israel, for a binational India–Israel grant. We are grateful to the Bar-Ilan research authorities for supporting this project. We thank Professor M. Deutsch for use of the x-ray diffraction facilities and Professor S. Margel and co-workers for their help in the TG-DSC measurements. We thank Dr. Yu. Kolytin and G. Kataby for their help in this investigation.

This work is a contribution of the National Institute of Standards and Technology, not subject to copyright.

- <sup>1</sup>T. R. Anantharaman, *Metallic Glasses* (Trans Tech, Aedermannsdorf, Switzerland, 1984).
- <sup>2</sup>P. Haasen and R. I. Jaffe, *Amorphous Metals and Semiconductors* (Pergamon, London, 1986).
- <sup>3</sup>N. F. Motte and E. A. Davis, *Electronic Processes in Non-Crystalline Materials* (Clarendon, Oxford, 1979).
- <sup>4</sup>H. Steeb and H. Warlimont, *Rapidly Quenched Metals* (Elsevier, Amsterdam, 1985).
- <sup>5</sup>T. Egami, Rep. Prog. Phys. **47**, 1601 (1984).
- <sup>6</sup>I. A. Abrikosov, O. Eriksson, P. Söderlind, H. L. Skriver, and B. Johansson Phys. Rev. B **51**, 1058 (1995).
- <sup>7</sup>V. L. Moruzzi, Solid State Commun. **83**, 739 (1992).
- <sup>8</sup>K. S. Suslick, Science **247**, 1439 (1990).
- <sup>9</sup>E. B. Flint and K. S. Suslick, Science **253**, 1397 (1991).
- <sup>10</sup>A. A. Atchley and L. A. Crum, in *Ultrasound, Its Chemical, Physical and Biological Effects*, edited by K. S. Suslick (VCH, New York, 1988).
- <sup>11</sup>A. L. Greer, Science **267**, 1947 (1995).
- <sup>12</sup>K. S. Suslick, D. A. Hammerton, and R. E. Cline, Jr., J. Am. Chem. Soc. **108**, 5641 (1986).
- <sup>13</sup>K. S. Suslick, S.-B. Choe, A. A. Cichowlas, and A. A. Grinstaff, Nature (London) **353**, 414 (1991).
- <sup>14</sup>M. W. Grinstaff, M. B. Salamon, and K. S. Suslick, Phys. Rev. B **48**, 269 (1993).
- <sup>15</sup>K. S. Suslick, M. Fang, T. Hyeon, and A. A. Cichowlas, in *Molecularly Designed Nanostructured Materials*, edited by K. E. Gonsalves (Materials Research Society, Pittsburgh, 1994).
- <sup>16</sup>R. Bellissent, G. Galli, T. Hyeon, S. Magazu, D. Majolino, P. Migliardo, and K. S. Suslick, Phys. Scr. **T57**, 79 (1995).
- <sup>17</sup>K. S. Suslick, T. Hyeon, and M. Fang, Chem. Mater. **8**, 2172 (1996).
- <sup>18</sup>K. S. Suslick, T. Hyeon, M. Fang, and A. A. Cichowlas, Mater. Sci. Eng. A **204**, 186 (1995).
- <sup>19</sup>Yu. Koltypin, G. Katabi, X. Cao, R. Prozorov, and A. Gedanken, J. Non-Cryst. Solids **201**, 159 (1996).
- <sup>20</sup>X. Cao, Yu. Koltypin, G. Katabi, R. Prozorov, and A. Gedanken, J. Mater. Res. **10**, 2952 (1995).
- <sup>21</sup>X. Cao, R. Prozorov, Yu. Koltypin, G. Katabi, I. Felner, and A. Gedanken (unpublished).
- <sup>22</sup>*Binary Alloy Phase Diagrams* (American Society for Metals, Metals Park, Ohio, 1986), Vol. 1, p. 1086.
- <sup>23</sup>C. E. Johnson, M. S. Ridout, T. E. Cranshaw, and P. E. Madsen, Phys. Rev. Lett. **6**, 450 (1961).
- <sup>24</sup>S. Morup, J. A. Dumesic, H. Topsøe, in *Applications of Mössbauer Spectroscopy*, edited by R. L. Cohen (Academic, New York, 1980), Vol. 2, p. 1.
- <sup>25</sup>K. S. Suslick, P. F. Schubert, and J. W. Goodale, J. Am. Chem. Soc. **103**, 7342 (1981).